

Application of laser ablation-ICP-MS to determine high-resolution elemental profiles across the Cretaceous/Paleogene boundary at Agost (Spain)

Claudia Sosa-Montes de Oca^{a,*}, Gert J. de Lange^b, Francisca Martínez-Ruiz^c,
Francisco J. Rodríguez-Tovar^a

^a Departamento de Estratigrafía y Paleontología, Universidad de Granada, Avda. Fuentenueva s/n, 18002 Granada, Spain

^b Department of Earth Sciences–Geochemistry, Geosciences, Utrecht University, 3584 CD, Utrecht, The Netherlands

^c Instituto Andaluz de Ciencias de la Tierra, IACT (CSIC-Universidad de Granada), Avda. Las Palmeras 4, 18100 Armilla, Granada, Spain

ARTICLE INFO

Keywords:

LA-ICP-MS

Resin-embedding

KPgB

Ejecta layer

Bio-events

Trace-element remobilization

ABSTRACT

A high-resolution analysis of the distribution of major and trace elements across a Cretaceous/Paleogene boundary (KPgB) was done using Laser Ablation-Inductively Coupled Plasma-Mass Spectrometry (LA-ICP-MS) and was compared with traditional distinct sampling and analysis. At the Agost site (SE Spain) a 22-cm-long core containing the KPgB was recovered using a Rolatec RL-48L drill. Within this interval, the lowermost 5 cm correspond to the Maastrichtian and the uppermost 17 cm to the Danian. The core section was resin-embedded under O₂-free conditions, cut and polished for LA-ICP-MS continuous measurements with 10 µm increments and a laser-beam of 80 µm. Elemental concentrations in discrete samples taken prior to embedding from the same core interval were determined by Inductively Coupled Plasma-Optical Emission Spectroscopy (ICP-OES). The LA-ICP-MS analyses in continuous mode considerably improve the resolution of geochemical profiles, allowing the compositional variability at a micrometer scale within the ejecta layer to be detected. In this study, we obtained profiles with 255 data points for the ejecta layer interval compared to 3 data points obtained by traditional manual sampling and ICP-OES analyses. Yet our recovered core section showed a rather limited preservation of the ejecta layer. This paper focuses on the presentation of LA-ICP-MS analysis as a particularly useful tool to investigate paleoenvironmental changes associated with bio-events. Additionally, the high-resolution of major and trace elemental distribution made it possible to study remobilization across thin but distinct boundaries such as the KPgB.

1. Introduction

Appropriate analytical resolution is crucial for paleoenvironmental studies based on geochemical proxies, in particular for those involving lithological boundaries as is the case of the KPgB. In general, data resolution has increased in recent decades in the wake of advanced capabilities and new analytical techniques. One of these new techniques is LA-ICP-MS (e.g., [Sylvester and Jackson, 2016](#)). This set-up combines novel developments over the past 30 years, involving laser ablation systems and elemental analytical methodologies at sub-mm resolution. As a result, LA-ICP-MS permits high-resolution elemental analysis including several continuous diagnostic trace elements at the sub-mm scale. LA-ICP-MS has been successfully applied in different scientific fields, such as: detailed analysis of natural rock systems ([Jenner and Arevalo, 2016](#)); microanalysis of fluid inclusions in hydrothermal systems ([Wagner et al., 2016](#)); and high-frequency variability in

unconsolidated Holocene sediments ([Jilbert et al., 2008](#)).

The technique therefore allows high-resolution analyses within layers of sub-mm thickness, as is the case for the KPgB at distal sections ([Urrutia-Fucugauchi and Pérez-Cruz, 2016](#)). This boundary, dated at 66.04 ± 0.02 Ma ([Renne et al., 2013](#)), has been widely studied ([Goderis et al., 2013](#); [Schulte et al., 2010](#)), and its link to a meteorite impact broadly demonstrated ([Alvarez et al., 1980](#); [Schulte et al., 2010](#); [Smit and Hertogen, 1980](#)). The impact caused major environmental changes (e.g., [Kring, 2007](#); [Wilf et al., 2003](#)), including an impact winter ([Brugger et al., 2017](#); [Vellekoop et al., 2014](#); [Woelders et al., 2017](#)), followed by global warming ([Vellekoop et al., 2014, 2016](#)) and ocean acidification (e.g., [Alegret et al., 2012](#); [Alegret and Thomas, 2005](#); [Peryt et al., 2002](#)). In addition, it produced tsunamis and related deposits not only in the immediate vicinity of the Chicxulub impact area ([Shonting and Ezrailson, 2017](#)), but also at sites as distal as Argentina ([Scasso et al., 2005](#)), Bulgaria ([Preisinger et al., 2002](#)), Croatia

* Corresponding author.

E-mail addresses: csosa@ugr.es, esm@iact.ugr-csic.es (C. Sosa-Montes de Oca), G.J.deLange@uu.nl (G.J. de Lange), fmruiz@ugr.es, fmruiz@iact.ugr-csic.es (F. Martínez-Ruiz), fjrtovar@ugr.es (F.J. Rodríguez-Tovar).

<https://doi.org/10.1016/j.palaeo.2018.02.012>

Received 2 October 2017; Received in revised form 9 February 2018; Accepted 9 February 2018

Available online 13 February 2018

0031-0182/ © 2018 Elsevier B.V. All rights reserved.

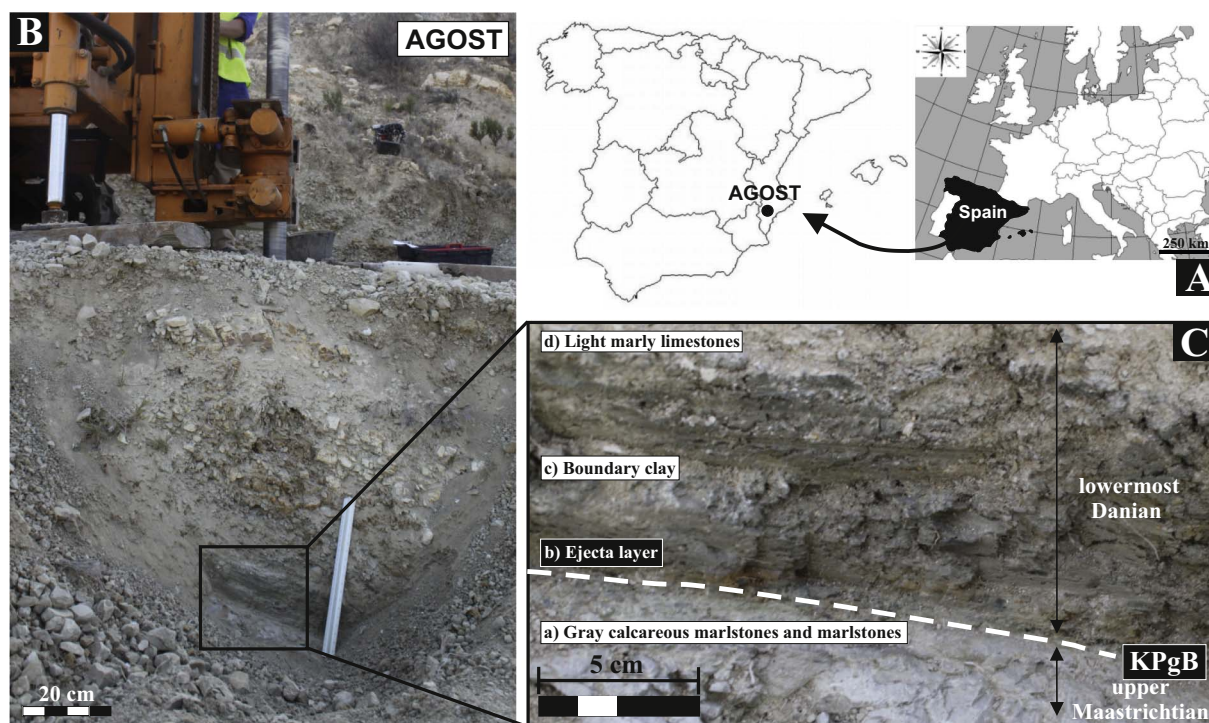


Fig. 1. Agost outcrop.

A) Location of the Cretaceous–Paleogene transitions (KPgT) at Agost site (Alicante, Southeast Spain). B) Close photographs during drilling. C) The Agost KPgT comprises by: (a) gray calcareous marlstones and marlstones from the uppermost Maastrichtian, (b) 2–3 mm thick ejecta layer, (c) blackish-gray boundary clay layer and (d) the light marly limestones, the last three belonging to the lowermost Danian.

–(Korbar et al., 2015), and The Netherlands –(Brinkhuis and Smit, 1996).

Major geochemical anomalies, recognized worldwide, characterize this boundary in both marine and continental depositional environments (Goderis et al., 2013). The extraterrestrial contribution is particularly evident in the ejecta layer of marine distal sites, located > 4000 km away from the Chicxulub impact crater (Goderis et al., 2013; Smit, 1999; Urrutia-Fucugauchi and Pérez-Cruz, 2016). In contrast, at marine proximal or intermediate sites, located closer to the impact site—such as Blake Nose (Martínez-Ruiz et al., 2001) or Demerara Rise (Berndt et al., 2011)—the extraterrestrial metal contribution is highly diluted by target rocks.

Recently, LA-ICP-MS analysis was used to study the geochemistry and textural characteristics of glass spherules in proximal (Belza et al., 2015; Ritter et al., 2015) and distal sites (Belza et al., 2017) and LA-ICP-MS analyses have furthermore been undertaken in intermediate sites of KPgB (Berndt et al., 2011; Lorocho et al., 2016), but merely oriented towards the analysis of individual spots, not in the continuous high-resolution laser mode as used here.

The Agost site (SE Spain) is one of the best-preserved and well-exposed marine distal settings of the KPgB (Macleod and Keller, 1991). It has been intensely studied because of its exceptional, expanded and continuous sedimentary record across the KPgB, i.e. without a hiatus (Molina, 2015; Rodríguez-Tovar et al., 2006). Hence, the Agost site is ideal for high resolution studies.

Nevertheless, appropriate high-resolution sampling is a challenge across the KPgB, due to the nature of the deposit, being a consolidated Maastrichtian gray calcareous marlstone and marlstone followed by the loose and unconsolidated ejecta layer and boundary clay, overlain by Danian light marly limestones. Furthermore, the thickness (millimetric scale) of the ejecta and boundary clay layers makes the in-tact sampling of a section containing all units extremely difficult. For this study, the KPgB at the Agost site was drilled using a Rolatec RL 48L drilling machine.

We present here the first high-resolution continuous analysis (μm -scale) of Ca/Al, P/Al, Sr/Al, Ti/Al, Cr/Al, Co/Al, Cu/Al, Zr/Al, Pb/Al and U/Al ratios using LA-ICP-MS after resin embedding across the KPgB at Agost. The results of our novel methodology are compared with those obtained by means of traditional sampling and ICP-OES analysis, and show how sub-mm peaks remain undetected by traditional analysis. Such peaks are potentially diagnostic for diverse processes including diagenesis.

2. Geological setting

The KPgB distal section of Agost ($38^{\circ}27'3.31''\text{N}$; $0^{\circ}38'9.71''\text{E}$), located at km 9 on the west side of road CV-827, north of the town of Agost, Alicante (Spain), at 372.3 m altitude, was drilled for a high resolution study (Fig. 1).

The Agost site was at a distance of 5600 km from the Chicxulub impact structure at.

the time of deposition and is thus considered a distal section (e.g., Goderis et al., 2013; Urrutia-Fucugauchi and Pérez-Cruz, 2016); it is thought to represent a paleo-deposition depth of ~600–1000 m (Alegret and Thomas, 2013; Smit, 1990), an upper-middle-bathyal environment similar to or slightly shallower than that proposed for the nearby Caravaca site.

In ascending order, the Agost Cretaceous–Paleogene transition comprises: (a) the Cretaceous sediments that consist of gray calcareous marlstones and marlstones from uppermost Maastrichtian age, overlain by Paleogene sediments that include: (b) the 2–3-mm-thick red clay (the ejecta layer), (c) a blackish-gray clay layer (the boundary clay) that has gradually increasing carbonate contents, related with the recovery of biological productivity, giving way to the typical (d) light marly limestones from the lowermost Danian age (Fig. 1). The ejecta layer, marking the sharp contact between the Maastrichtian and Danian (KPgB), contains impact evidence such as spherules, Ir and other platinum-group element anomalies as well as enhanced concentrations of

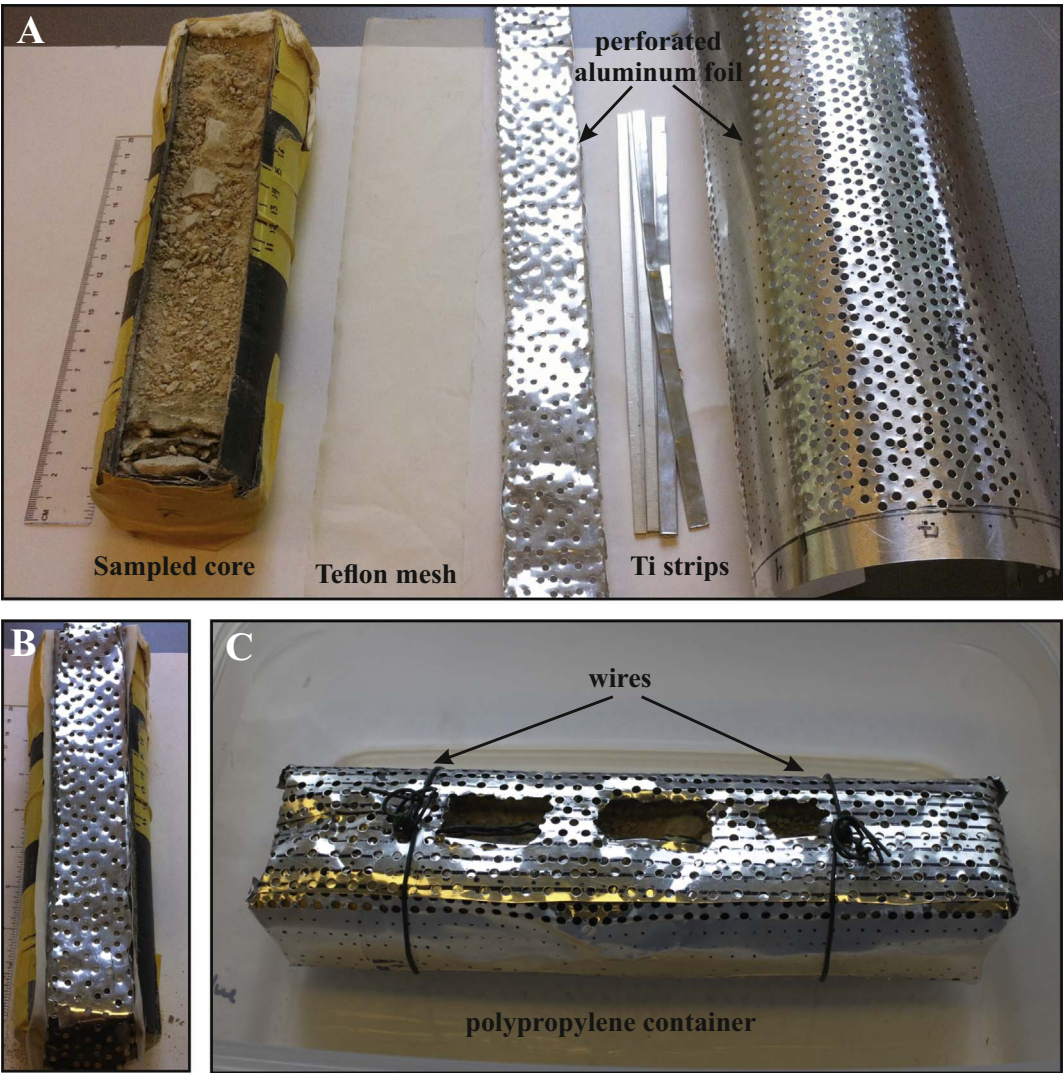


Fig. 2. Material used in the preparation of the core prior to the resin embedding process.

Table 1
Components of formulations of Spurr epoxy resin and relative masses.

Spurr epoxy resin	Code	Relative mass
Cycloaliphatic epoxide resin	ERL 4221	16.4
Diglycidal ether of polypropyleneglycal	DER 736	5.72
Nonenyl succinic anhydride	NSA	23.6
Dimethylaminoethanol	DMAE	0.40

further trace elements such as Cr, Co, Ni, Cu, Zn, As and Sb. In addition, this interval registers a significant decline in planktonic $\delta^{13}\text{C}$ values, related to the decrease in primary productivity, and a decrease of $\delta^{18}\text{O}$ values related to T^{a} variations (Goderis et al., 2013; Smit, 1990; Schulte et al., 2010).

The Agost site has been broadly studied in terms of mineralogical (i.e. Ortega-Huertas et al., 2002, 1995), geochemical and isotopic composition (i.e. Ibáñez-Insa et al., 2017; Martínez-Ruiz et al., 1999; Ortega-Huertas et al., 1995, 1994; Rodríguez-Tovar et al., 2006, 2004), ichnological analysis (Laska et al., 2017; Rodríguez-Tovar, 2005; Rodríguez-tovar and Uchman, 2004a, 2004b) and biostratigraphical studies, based on planktonic and benthic foraminifers (i.e. Arenillas et al., 2004; Arz et al., 2000; Canudo et al., 1991; Molina, 2015; Molina et al., 2005, 1998, 1996).

3. Materials and methods

3.1. Coring

Due to the difficulty in recovering a fresh/unexposed and in-tact sample of the full KPgB interval, containing the 4 parts mentioned above, from the uppermost Maastrichtian to the lowermost Danian, a bore hole was drilled to obtain a core with the complete transition. It was recovered using a Rolatec RL 48 L drilling machine with rubber tracks from the Center for Scientific Instrumentation (CIC), University of Granada, Spain (Fig. 1 in data in brief, Sosa-Montes de Oca et al., in press).

From the platform for the drilling machine, the depth to the KPgB was estimated based on a nearby excavation. Subsequently drilled was till approximately 30 cm above the boundary, and an unaltered core sample was extracted by introducing an open thick-walled sampler, and hitting this with a mallet of 63.5 kg until a maximum of 75 cm penetration (size of walled sampler). Within this sampler a PVC tube is inserted, so that our targeted sediment interval was recovered inside the PVC tube (Fig. 2). Once obtained, the core was sealed and stored in a cold room.

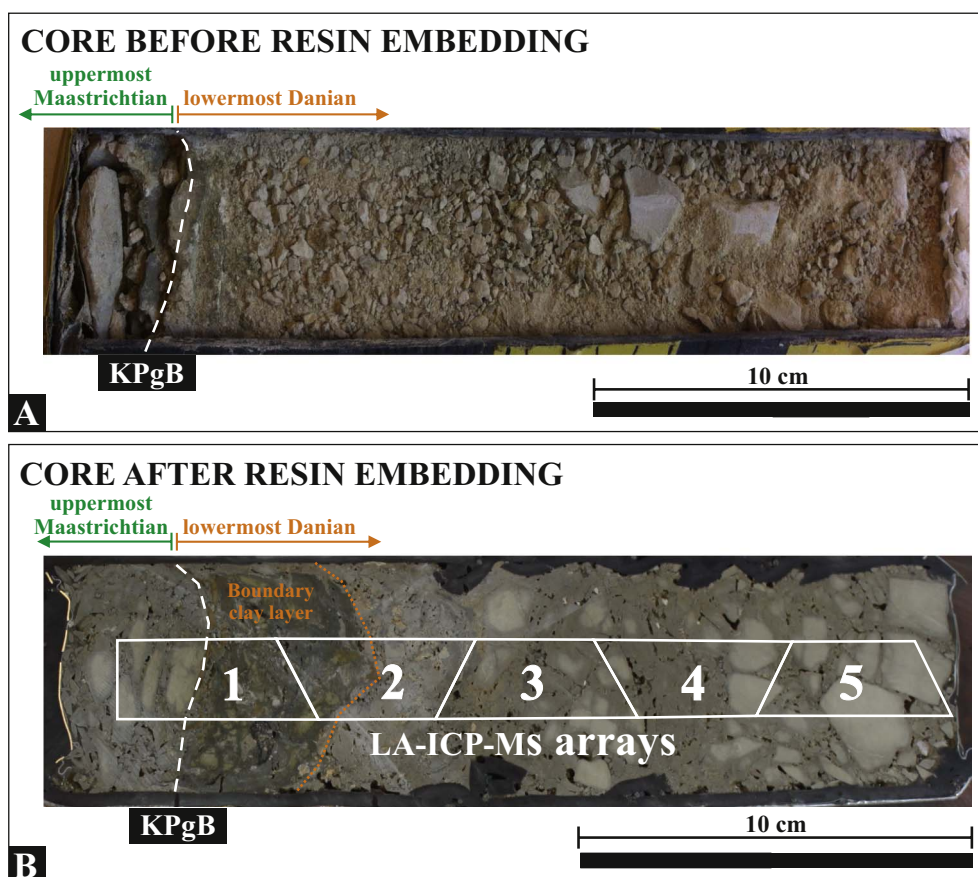


Fig. 3. Close photographs of studied core before and after resin embedding process.

i) Core before resin embedding consolidation (Panel A).

ii) Core after resin embedding consolidation where the arrays made for LA-ICP-MS measurements are marked (Fig. 3B).

3.2. Resin embedding of the KPgB interval

For resin-embedding, the PVC tube containing the partly unconsolidated material was placed horizontal, and a strip of the PVC was carefully cut and removed (Fig. 2A). Discrete samples were taken for ICP-OES analyses. As PVC does not resist the attack with acetone needed for the resin-embedding, the core was enforced using 0.2 mm aluminum foil. To do so, first the exposed sediment was covered with a teflon mesh (dimensions 240×30 mm) and perforated aluminum foil (dimensions 240×30 mm) (Fig. 2B), and finally all was covered with perforated aluminum foil (dimensions 240×190 mm), fixing it with wires (Fig. 2C).

Spurr Epoxy Resin was used for resin embedding (see Jilbert et al., 2008), through which we not only preserve redox-sensitive elements, but also maintain the material structure. All the processes were performed in an argon-filled glove box during 32 days, in two different stages. The first was with acetone alone, for 5 consecutive days. To this end, 2 L of oxygen-free acetone were used, changing them every 24 h and keeping the core always submerged (Fig. 2 in data in brief, Sosa-Montes de Oca et al., 2017). At the same time and also inside the anoxic glove box, small pieces of PVC were immersed in a small batch of acetone to analyze the potential contamination this might produce. The contamination was tested with ICP-OES analyses, and appeared to be insignificant. The second stage entailed Spurr Epoxy Resin exchange (Table 1) during 27 days, in which 4 sub-steps were differentiated: Step 1: using a mixture of acetone and resin (3:1; 75% acetone: 25% resin) for 7 days. Step 2: using a mixture of acetone and resin (2:1; 66% acetone: 33% resin) for 7 days. Step 3: using a mixture of acetone and resin (1:1; 50% acetone: 50% resin) for 7 days. By last, step 4: using

pure Spurr Epoxy Resin for 6 days. All exchanges were done using syringes with the core remaining undisturbed inside the bath.

After that, the core was removed from the glove box, put into the oven for cure and drying during 48 h at 60°C , and finally the solid resin core was cut perpendicular to the sedimentation plane (Fig. 3 in data in brief, Sosa-Montes de Oca et al., 2017). The surface was polished and cut to form 5 overlapping arrays (~ 5 cm), which were analyzed using LA-ICP-MS line-scan analysis (see Fig. 3).

3.3. LA-ICP-MS measurements and processing

Three line-scan analyses (a-b-c) for each of the arrays 1, 2, 3, 4 and 5 were performed. Exceptionally, for array 1, a total of 9 line-scan analyses (a-b-c-d-e-f-g-h-i) (see Fig. 4) were done. In this paper we report only the results from a line that includes the array 1 profile b and array 2 profile c, which was least affected by cracks. This line was of 84 mm and the measurements were taken at $10\mu\text{m}$ steps. For that distance 4414 values were obtained, including 544 data points in the gray calcareous marlstones and marlstones from the uppermost Maastrichtian, and 3570 data points from the lowermost Danian sediments. The latter breaks down to 255 data points taken in the ejecta layer, 1827 data points taken in the boundary clay layer, and 1488 data points taken in the light marly limestones from Danian (Supplementary material in data in brief, Sosa-Montes de Oca et al., 2017).

A 193 nm wavelength COMPex 102 ArF excimer laser ablation system (Lambda Physik, Göttingen, Germany) connected to an Element 2 sector field ICP-MS (Thermo Scientific, Bremen, Germany) was used for all LA-ICP-MS analyses at the GML from Utrecht University (the Netherlands). The use of a deep ultra-violet (193 nm) laser beam has

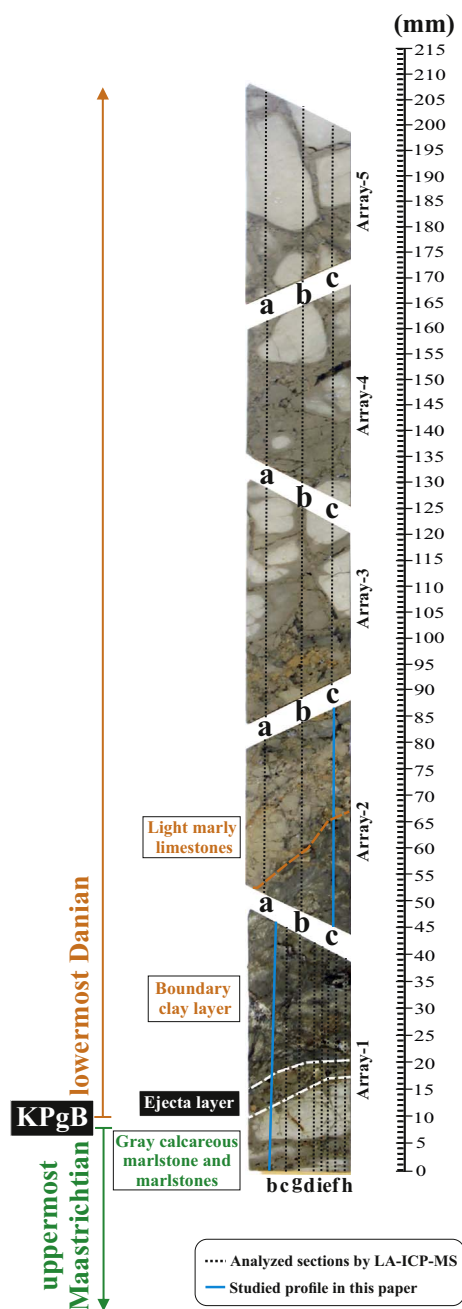


Fig. 4. LA-ICP-MS profiles.

Shown with dash line are all the profiles analyzed by LA-ICP-MS (Array-1, profiles b–c–d–e–f–g–h–i–j; array-2, profiles a–b–c; array-3, profiles a–b–c; array-4, profiles a–b–c and array-5, profiles a–b–c). With continuous blue line is the profile studied in this paper (array 1b–array 2c). (For interpretation of the references to color in this figure legend, the reader is referred to the web version of this article.)

been proven to significantly reduce elemental fractionation effects during the ablation process when compared to infrared lasers (Günther et al., 1998). The ICP-MS was operated at low mass resolution ($M/\Delta M = 400$) to provide optimal detection capability and sensitivity of the ICP-MS. The measurement frequency of the ICP-MS for all isotope spectra was ~ 2.5 – 3 Hz.

The 5 arrays obtained after resin embedding were analyzed and the data were processed following the procedure of Hennekam et al. (2015). In short, each array obtained was placed into a He-flushed ablation chamber for LA-ICP-MS analysis. For line-scanning the ablation chamber was moved perpendicular to the laminations of the resin-embedded arrays, at a speed of 0.0275 mm s^{-1} . The laser parameters

were kept constant at a pulse repetition rate of 10 Hz, spot diameter of $80 \mu\text{m}$, and energy density of $\sim 8 \text{ J cm}^{-2}$. Laser input at the ablation site (fluence) was monitored daily before tuning the ICP-MS for optimal sensitivity following the procedure of Wang et al. (2006). The measurement frequency and scanning rate resulted in a constant shift increment of $\sim 10 \mu\text{m}$ per measurement. When added to the laser spot diameter, this resulted in an overall sampled interval of $\sim 90 \mu\text{m}$ per ICP-MS cycle, having $80 \mu\text{m}$ overlap with the previous and subsequent measurements.

The obtained counts were evaluated, corrected for background noise, and calibrated. First the mean background values, obtained from the mean intensities of an $\sim 30 \text{ s}$ interval before the start of the laser ablation measurement, were subtracted from the raw analyte intensities. Subsequently the background-corrected analyte intensities were corrected for the relative sensitivity of the specific isotope calculated by measurement of an external standard (NIST SRM610, Jochum et al., 2011), and also corrected for the natural abundance following Berglund and Wieser (2011). As the yield of ablated material varies during LA-ICP-MS, data are commonly reported as ratios of the analyzed element to an internal standard. In our case the internal standard was Al. It is important to note that LA-ICP-MS line-scanning gives qualitative data.

Final data are presented as ratios because on μm - to mm -scales no internal standard with a known concentration is available during LA-ICP-MS line-scanning of natural samples. The profiles were made with log-ratios to avoid the asymmetrical properties of normal ratios (Aitchison and Egozcue, 2005). Subsequently, data were plotted using a moving average with 5 data (in blue color) and also with 10 data (in black) (see Fig. 5).

As a summary, LA-ICP-MS specifications as well as elemental ratios used in this paper are indicated in Table 2.

3.4. ICP-OES analyses

Prior to resin embedding, discrete samples were taken for analysis by ICP-OES. Specifically, 55 samples were taken along 22 cm of the KPgB transition; they included 10 samples in the 5 cm of gray calcareous marlstone and marlstone from the uppermost Maastrichtian, and 45 samples in the 17 cm of the lowermost Danian sediments (Table 1 in data in brief, Sosa-Montes de Oca et al., 2017). Of the latter, 3 samples were taken in the 0.50 cm of the ejecta layer, 18 samples taken in the 4.50 cm of the boundary clay layer, and 24 samples taken in the 12.00 cm of light marly limestone. The sampling resolution rates were of 0.15 cm in the ejecta layer, 0.25 cm for the samples from the boundary clay layer, and 0.50 cm for calcareous marlstone and marlstone samples from the uppermost Maastrichtian and light marly limestone samples from the lowermost Danian.

Prior to ICP-OES analyses, samples were totally digested following routine procedures (Reitz et al., 2006). Major and minor elements were measured with a Spectro Ciros Vision ICP-OES at the Geolab of Utrecht University (the Netherlands). Analytical precision and accuracy for ICP-OES were better than 5% for the measured elements.

The sediments across the KPgB display large oscillations in carbonate content, hence Al-normalized concentrations or recalculation on a carbonate-free basis were needed to reflect oscillations in elemental content and to avoid such a ‘closed sum’ effect (e.g. (Calvert and Pedersen, 1993; Tribouillard et al., 2006; van Os et al., 1991). The ratios analyzed using ICP-OES were P/Al, Ca/Al, Sr/Al, Ti/Al, Cr/Al, Co/Al, Cu/Al, Zr/Al, and Pb/Al (Table 1 in data in brief, Sosa-Montes de Oca et al., 2017).

3.5. High resolution scanning electron microscopy (HRSEM)

Textural and compositional information was also obtained from High Resolution Scanning Field Scanning Electron Microscope (HRSEM), the AURIGA from Carl Zeiss SMT. The HRSEM is located at

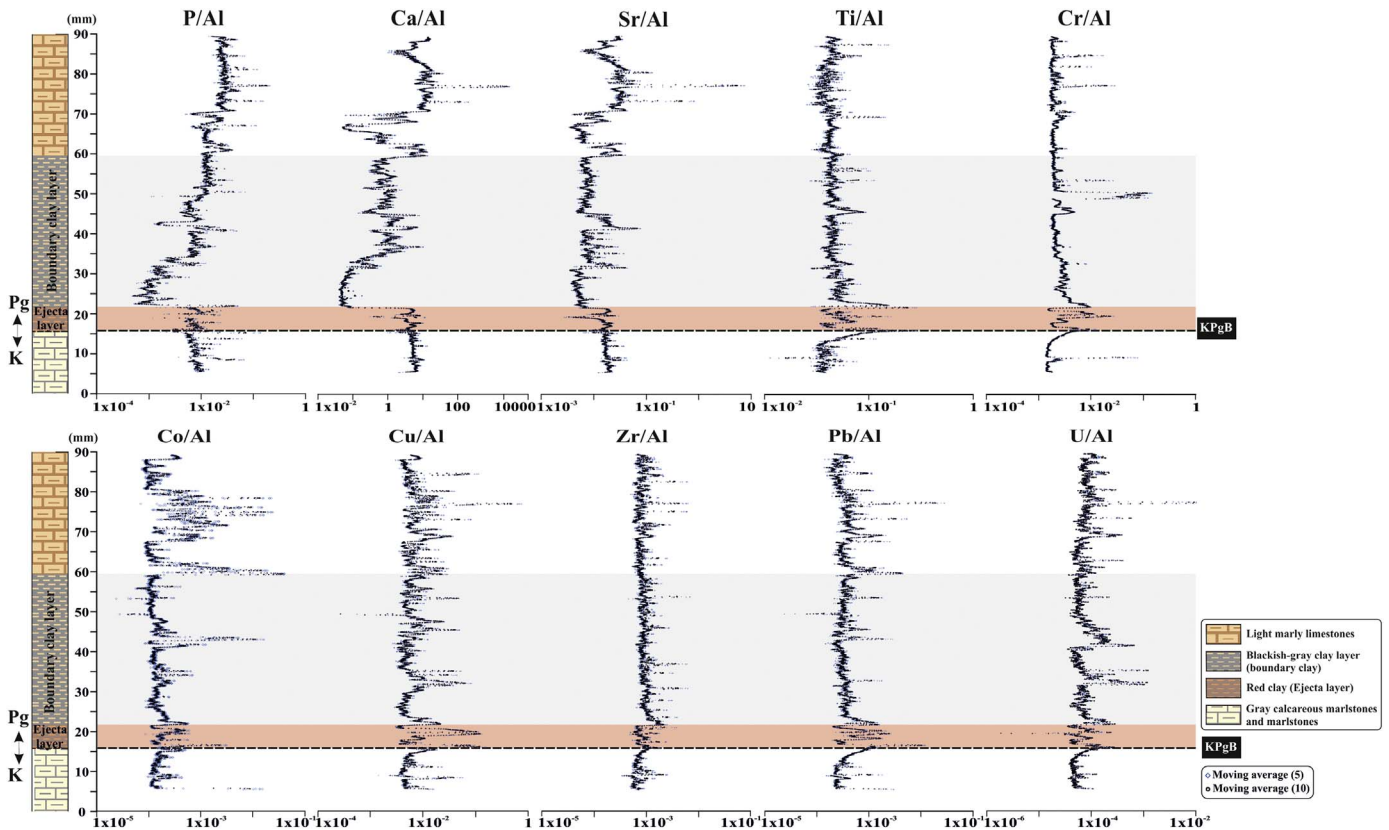


Fig. 5. Profiles by LA-ICP-MS. Elemental isotopic ratios measured by LA-ICP-MS across the KPgT at the Agost site. Ca/Al, P/Al, Sr/Al, Ti/Al, Cr/Al, Co/Al, Cu/Al, Zr/Al, Pb/Al and U/Al ratios; in i) the gray calcareous marlstones and marlstones from the uppermost Maastrichtian, ii) the ejecta layer, iii) the boundary clay layer and iv) the light marly limestones from the lowermost Danian.

Table 2
Typical LA-ICP-MS settings for measurements on resin embedded samples.

ICP-MS type	Thermo scientific element 2
RF power	1300 W
Plasma gas	Ar (16.00 l min ⁻¹)
Auxiliary gas	Ar (0.85 l min ⁻¹)
Carrier gas	Ar (0.67 l min ⁻¹) and He (0.75 l min ⁻¹)
Skimmer cone	Aluminum
Sampler cone	Nickel
Measurement frequency	~2.5–3 Hz
Resolution	Low (M/ΔM = 400)
Isotopes ^a	²³ Na, ²⁴ Mg, ²⁵ Mg, ²⁶ Mg, ²⁷ Al, ²⁹ Si, ³¹ P, ⁴³ Ca, ⁴⁴ Ca, ⁴⁹ Ti, ⁵¹ V, ⁵² Cr, ⁵⁵ Mn, ⁵⁷ Fe, ⁵⁹ Co, ⁶⁰ Ni, ⁶⁵ Cu, ⁶⁶ Zn, ⁷⁵ As, ⁷⁹ Br, ⁸¹ Br, ⁸⁸ Sr, ⁸⁹ Y, ⁹⁰ Zr, ⁹⁷ Mo, ⁹⁸ Mo, ¹⁰¹ Ru, ¹⁰³ Rh, ¹⁰⁵ Pd, ¹²¹ Sb, ¹³⁷ Ba, ¹⁴⁰ Ce, ¹⁸⁵ Re, ¹⁹³ Ir, ¹⁹⁴ Pt, ¹⁹⁵ Pt, ²⁰⁸ Pb, ²³² Th, ²³⁸ U
Laser type	COMPex 102 (ArF Excimer, Lambda Physik)
Wavelength	193 nm
Fluence	8 J cm ⁻²
Spot size diameter	80 μm
Repetition rate	10 Hz
Scanning rate	0.0275 mm s ⁻¹

^a Elements used in this paper.

the Center for Scientific Instrumentation (CIC), University of Granada (Spain). The analysis by HRSEM was focused on the KPgB, explicitly on the boundary between the gray calcareous marlstone and marlstone from the uppermost Maastrichtian and the ejecta layer from the lowermost Danian.

4. Results and discussion

4.1. Technical analytical results

Geochemical data and profiles of the line (Array1b–Array2c) analyzed by LA-ICP-MS are represented in supplementary material (in data in brief, Sosa-Montes de Oca et al., 2017) and Fig. 5 respectively. Geochemical data and profiles of the same core section but analyzed by ICP-OES on discrete samples are presented in Table 1 (in data in brief, Sosa-Montes de Oca et al., 2017) and Fig. 6 respectively.

4.2. Comparing discrete-samples ICP-OES vs continuous LA-ICP-MS analyses

The shared interval covered by discrete sampling/ICP-OES and by continuous/LA-ICP-MS analyses is 84 mm, including 10 mm of Maastrichtian gray calcareous marlstone and marlstone, 5 mm of the ejecta layer, 38 mm of the boundary clay, and 31 mm of light marly limestone from the lowermost Danian. The ejecta layer is commonly 0.2–0.3 mm thick at distal sections and has low carbonate content (Smit, 1999). Yet our recovered core section showed a rather limited preservation of the ejecta layer. This core disturbance became evident in the secondary electron images obtained with HRSEM (Fig. 7). The ejecta layer appears irregular and poorly preserved, and it contains small unaltered Maastrichtian limestone fragments. Although tsunami-generated disturbances have been reported in many distal sites (Brinkhuis and Smit, 1996; Korbar et al., 2015; Scasso et al., 2005), the consistently reported undisturbed sections at Agost do not support such process. In the profiles of Ca/Al, P/Al and Sr/Al, a significant decrease after the ejecta layer is observed, then a slight recovery along the boundary clay, reaching values similar to those of the uppermost Maastrichtian in

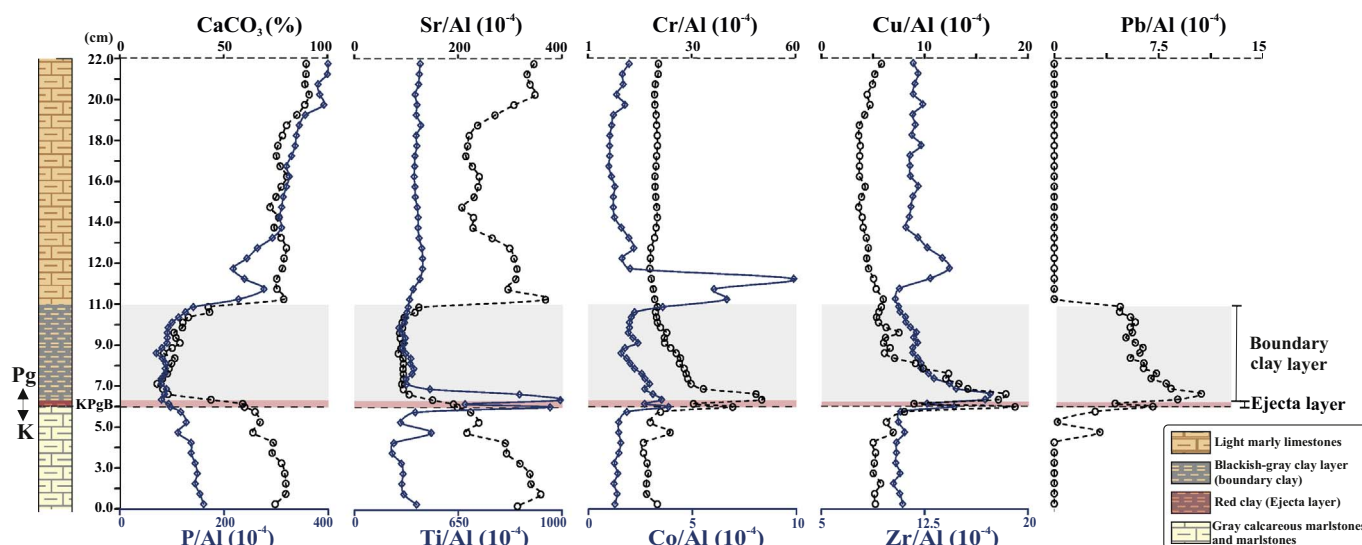


Fig. 6. Profiles by ICP-OES.

Elemental content (major and trace) and elemental ratios, measured by ICP-OES across the KPgB at the Agost site. Al, Ca, CaO, CaCO_3 , concentrations (%); Ca/Al and Fe/Al ratios; P/Al, Sr/Al, Ti/Al, Cr/Al, Co/Al, Cu/Al, Zr/Al and Pb/Al ratios ($\times 10^{-4}$), in i) the gray calcareous marlstones and marlstones from the uppermost Maastrichtian, ii) the ejecta layer, iii) the boundary clay layer and iv) the light marly limestones from the lowermost Danian.

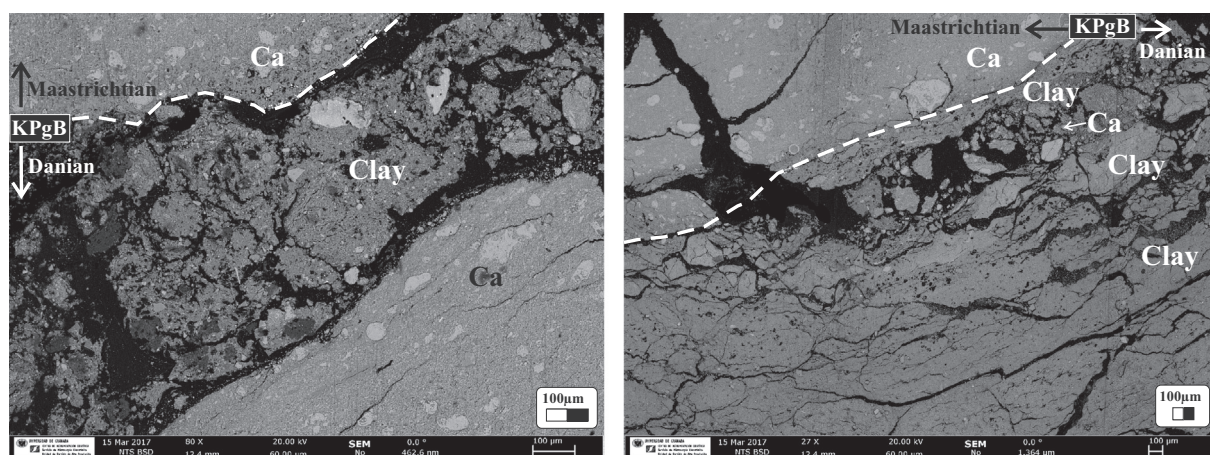


Fig. 7. Secondary electron images made by High Resolution Scanning Electron Microscopy (HRSEM). Visible is the fractured contact the between the gray calcareous marlstones and marlstones from the uppermost Maastrichtian and the ejecta layer from the lowermost Danian.

the light marls from the lowermost Danian. In contrast, elemental ratios as Ti/Al, Cr/Al, Co/Al, Cu/Al, Zr/Al, Pb/Al and U/Al show a clear peak at the KPgB (Figs. 5 and 6).

Specifically, when comparing the profiles obtained by both techniques (Fig. 8), we observe, for CaCO_3 (from ICP-OES Ca data) and the Ca/Al ratio analyzed by LA-ICP-MS, a maximum value of 75% CaCO_3 and 13 for Ca/Al ratio in the gray calcareous marlstone and marlstone from the uppermost Maastrichtian and in the light marly limestone from the lower Danian. Minimum values are observed for CaCO_3 (25%) and the Ca/Al ratio (0.05) at the base of the clay boundary, which gradually increases its carbonate content. Discordant data may at first sight be attributed to the difference in resolution between the two methods (Fig. 8).

Comparing the Ti/Al profile from ICP-OES and that from LA-ICP-MS, a large peak at the base of the ejecta layer (KPgB) was observed, but more peaks are also observed in the rest of the ejecta layer (Fig. 8).

No major changes in the profiles of redox sensitive elements such as Cr/Al, Co/Al, Cu/Al, Pb/Al and U/Al or in the profiles of detrital elements as Zr/Al were registered for the calcareous marlstone from uppermost Maastrichtian or the clay boundary from lowermost Danian. This is interpreted as evidence of similar paleoenvironmental

conditions (oxygenation and/or sedimentary input) prior to and after the KPgB, owing to a rapid re-establishment of environmental conditions (Sosa-Montes de Oca et al., 2013, 2016, 2017).

Within the ejecta layer, due to its poor preservation, no clear correlation between the observed changes and the paleoenvironmental or diagenetic conditions is possible. Nevertheless, different peaks show the enormous potential of the applied methodology (LA-ICP-MS analyses in continuous mode after resin embedding) to investigate major and trace element distribution and remobilization (at sub-mm scale) across abrupt boundaries like the KPgB.

First, we compare the Cr/Al, Co/Al, Cu/Al, Zn/Al, Pb/Al and Ti/Al profiles obtained using the two techniques (ICP-OES and LA-ICP-MS), in a 3 mm interval (Fig. 9). Although Ni is also a typical meteorite-related element, we neither display nor discuss the Ni/Al profile, as it did not show clear peaks in this interval. Using discrete samples and the resulting limitations in sample resolution across an abrupt interval, commonly peaks of Cr, Co, Cu, Zn, Pb and Ti are reported to occur simultaneously. This is also observed for our discrete samples analyzed by ICP-OES. However, using LA-ICP-MS analysis several peaks are observed in a sub-mm scale. Titanium is an element usually taken to be immobile, whereas elements as Pb, Cr, Cu, Co and Zn may be mobile

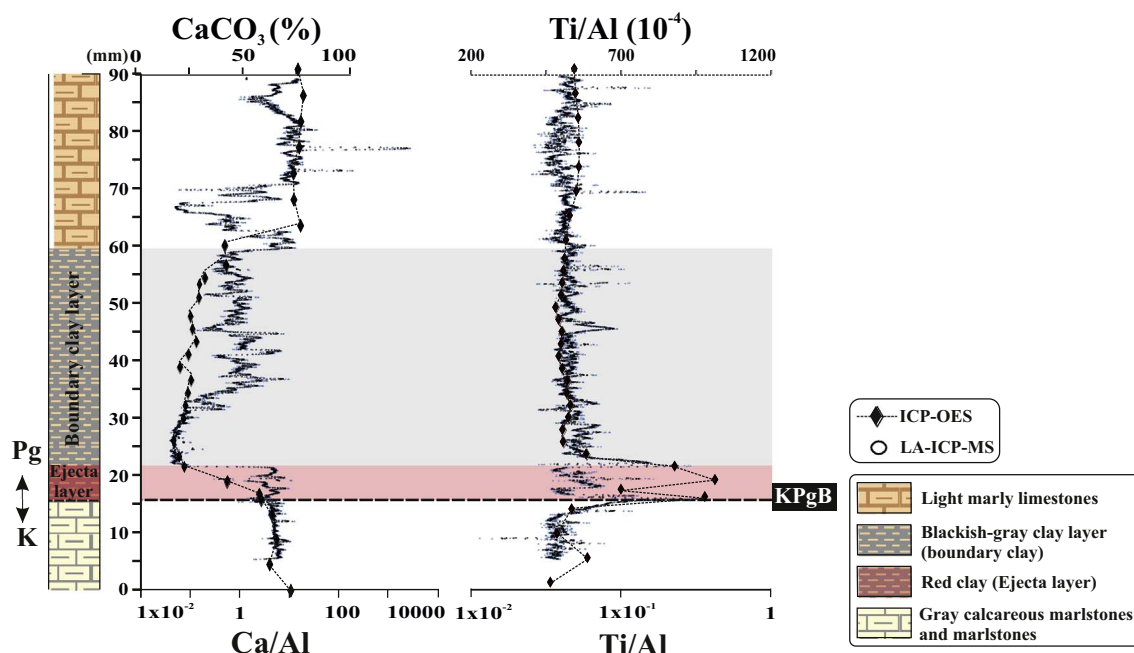


Fig. 8. Comparison of CaCO_3 (%) analyzed by ICP-OES vs Ca/Al ratio analyzed by LA-CP-MS, and Ti/Al (10^{-4}) analyzed by ICP-OES vs Ti/Al ratio analyzed by LA-CP-MS, both in a 9 mm interval, including: i) in the gray calcareous marlstones and marlstones from the uppermost Maastrichtian, ii) the ejecta layer, iii) the boundary clay layer and iv) the light marly limestones from the lowermost Danian.

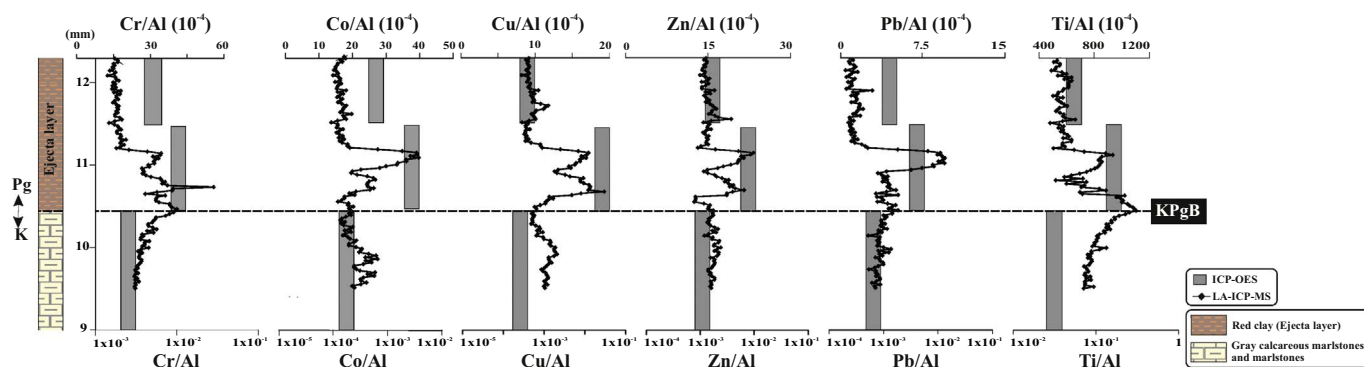


Fig. 9. Comparison of Cr/Al , Co/Al , Cu/Al , Zn/Al , Pb/Al and Ti/Al (10^{-4}) analyzed by ICP-OES vs the same ratios ratios analyzed by LA-ICP-MS, in a 3 mm interval, including: i) the gray calcareous marlstones and marlstones from the uppermost Maastrichtian and ii) the ejecta layer from the lowermost Danian.

under different redox conditions. Such fractional deposition or diagenetic mobilization of elements could be studied in the case of better preserved core material (Fig. 9).

The initial aim of this study was not only to demonstrate the novel high-resolution approach but also to apply this in a detailed reconstruction so as to assess the evolution of paleoenvironmental conditions (i.e., rate of oxygenation, nutrient availability, and sedimentary input). Unfortunately, an in-depth paleoceanographic interpretation of our data is not warranted. Consequently, this MS predominantly demonstrates that the applied methodology (LA-ICP-MS analyses in continuous mode after resin embedding) is adequate for advanced studies of abrupt boundaries such as the KPGB.

The first important observation is that peaks for different elements commonly coinciding in traditional mm/cm-resolution sampling, clearly do not all coincide at μm -sample resolution. This is essential for unravelling depositional versus diagenetic processes. Impact(s) may have resulted in the sequential deposition of typical impact-related material, whereas subsequent diagenetic processes may have resulted in the mobilization and sequential deposition of certain trace elements. Such sequential (re)deposition at abrupt boundaries like the KPGB is probably limited to the sub-mm scale, for which reason high resolution

tools are required to detect these processes.

4.3. Technical advantages provided by LA-ICP-MS

The obtained Ti-profile provides a clear example of the different capabilities of the two methodologies used here, i.e. discrete sampling followed by ICP-OES and continuous sub-mm scale analysis using LA-ICPMS. The Ti profile has a peak with a width of 1 mm by LA-ICP-MS (Fig. 5), while the same peak seems to cover 10 mm by ICP-OES (Fig. 6). Furthermore, at a sub-mm scale, the multiple peaks observed in the detailed profiles of Fig. 10 occur within a 1 mm interval. This can only be adequately detected using LA-ICP-MS, not using traditional discrete sampling. The obvious, main difference is the analytical resolution, being ~ 1 mm versus 0.09 mm. This represents, for the ~ 5 mm thick ejecta layer, that the amount of analytical data by LA-ICP-MS is much larger than by discrete sampling and ICP-OES: 255 versus 3 (Figs. 5 and 6). The low resolution obtained with traditional sampling, commonly limited to a resolution of 1 mm at best, could easily lead to missed or coinciding elemental peaks or other features. In contrast, the high resolution obtained with the continuous LA-ICP-MS analysis may lead to advanced and better interpretations, proving a particularly useful tool

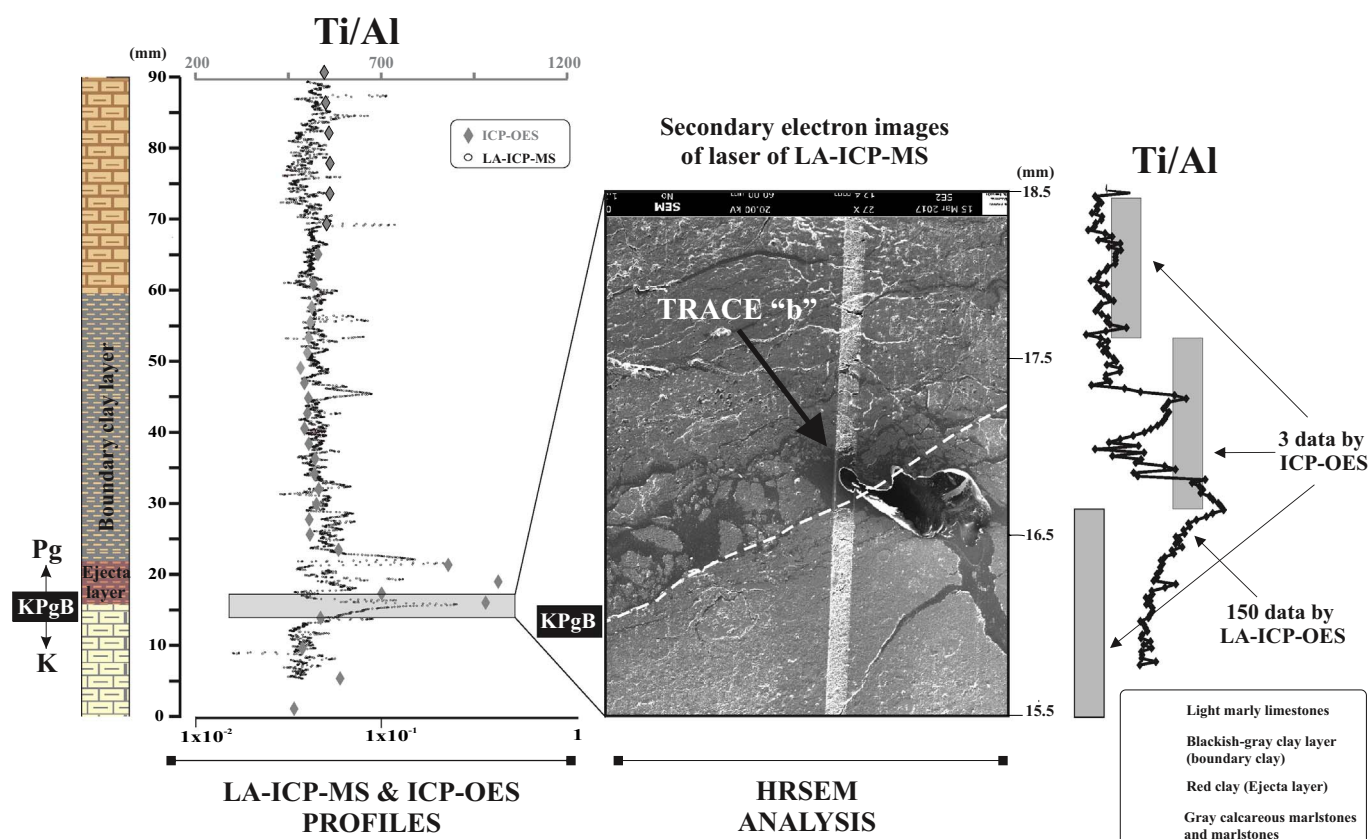


Fig. 10. Comparison of ICP-OES, LA-CP-MS and HRSEM.

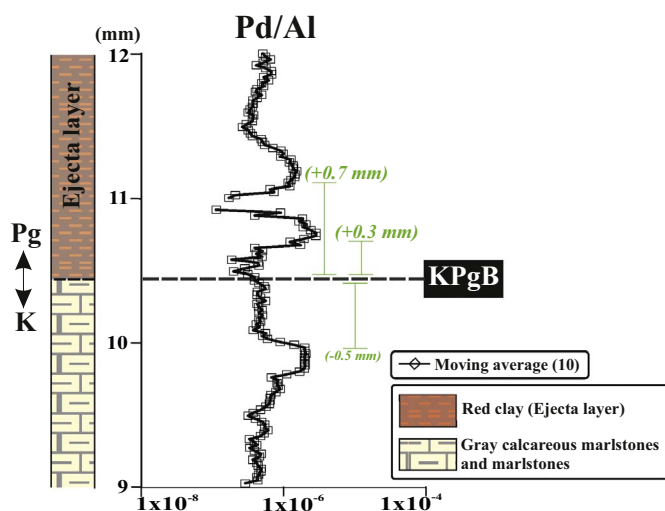


Fig. 11. Profile of Pd/Al ratio analyzed by LA-ICP-MS, in a 3 mm interval included in i) the gray calcareous marlstones and marlstones from the uppermost Maastrichtian and ii) the ejecta layer from the lowermost Danian.

to investigate element distribution and remobilization at a sub-mm scale.

Another useful and relevant example of high resolution results by LA-ICP-MS is observed in the Pd/Al profile (Fig. 11). Although the detection of Pd may be influenced by some isobaric interferences, several peaks are observed within a 3 mm interval. Hence, a distinct pattern with rapid sub-mm changes can be detected at the sub-mm resolution but cannot be observed by traditional discrete sampling and subsequent analysis by ICP-OES.

Other interesting elements in particular for the KPgB are Pt and Ir.

Yet due to their low sensitivity and the poor preservation of the ejecta layer in our core, both elements remained unquantified. The slightly enhanced level of Ir observed at the KPgB does, however, demonstrate the potential of our approach for Ir, and even more so if applied to an undisturbed KPgB with a thin but potentially more concentrated Ir-horizon. Alternatively, if remobilization of Ir, Pt, Pd or other PGE has occurred at this boundary, not only the peaks of these elements could be underestimated but also all calculation results derived from them. They include asteroid size, amount and nature of debris ejected, as well as the severe environmental effects produced. The high-resolution detection of these elements would therefore be advantageous for an adequate interpretation of all processes at the KPgB.

4.4. Application of LA-ICP-MS to the KPgB

Despite significant diagenesis and potential remobilization of certain elements, it has been demonstrated that the KPgB preserved the original signature for a range of elements within the ejecta layer, as evidenced by PGE anomalies (e.g., Martínez-Ruiz et al., 1999; Rodríguez-Tovar et al., 2006; Smit, 1990; Smit and Klaver, 1981) and also by the extraterrestrial nature of trace elements such as Cr (Shukolyukov and Lugmair, 1998). Furthermore, as documented by previous environmental studies carried out at this boundary, the impact event was responsible for main environmental perturbations including nitric and sulfuric acid rain, widespread dust and blackout, destruction of the stratospheric ozone layer, and an enhancement of the greenhouse effect (e.g., Kring, 2007). It also led to secondary effects such as an increase in oceanic acidification (e.g., Alegret et al., 2012; Alegret and Thomas, 2005; Peryt et al., 2002) and a decrease in the sea surface temperature (Galeotti et al., 2004; Kaiho et al., 2016; Vellekoop et al., 2015, 2014). Because such perturbations sharply transformed depositional and ecological conditions, the reestablishment of paleoenvironmental conditions after the KPgB is of special interest in the context of

evolutionary and ecological dynamics e.g., (Hull, 2015).

In general, the high resolution approach provided by LA-ICP-MS analyses, as opposed to ICP-OES (Fig. 10), enables researchers to verify the above information and moreover to reconstruct in detail the environmental changes associated with the recovery time of oxic conditions and productivity (Alegret et al., 2012; Alegret and Thomas, 2009; Birch et al., 2016; Esmeray-Senlet et al., 2015; Schueth et al., 2015; Sepúlveda et al., 2009; Sosa-Montes de Oca et al., 2017, 2016).

Comparing the traditional sampling done with ICP-OES analyses and the advanced approach with LA-ICP-MS, the major advance using the latter becomes evident: values for the transition from typical Maastrichtian to ejecta level are 10 mm for ICP-OES and 1 mm using LA-ICP-MS methodology. Expressed in time, and taking into account that the ejecta layer was deposited within a few days (up to a couple of weeks for the finest fractions) after the impact (Artemieva and Morgan, 2009), and that the lowermost Danian sedimentation rate is of 0.83 cm/ka (Groot et al., 1989), the 10 vs 1 mm results could indicate a somewhat different post-impact recovery time to oxic conditions (1200 versus < 1 year).

In sum, analyzing an adequate and well-preserved KPgB using the high-resolution LA-ICP-MS methodology described here will help improve our knowledge of the recovery time of oxic conditions and therefore biological productivity, while also shedding new light on depositional and diagenetic processes such as the remobilization of trace elements that are potentially associated with such an abrupt boundary.

5. Conclusions

High resolution analyses were performed on a distal section from the KPgB at the Agost site, southeastern Spain. Results obtained by traditional sampling and ICP-OES analysis were compared with a novel methodology, using resin-embedded sediment and LA-ICP-MS continuous measurements with 10 µm increments and a laser-beam of 80 µm. Due to the largely improved analytical resolution, sub-mm variability was observed that remained undetected while using traditional discrete sampling and ICP-OES analysis. Traditional sampling may easily lead to missed or coinciding elemental peaks, whereas the high resolution obtained with continuous LA-ICP-MS analysis permits advanced interpretations. The latter is particularly useful for investigating element distribution and remobilization (at sub-mm scale) across abrupt boundaries such as the Cretaceous-Paleogene boundary (KPgB). This will not only improve our knowledge surrounding the recovery time of oxic conditions thus biological productivity, but will also be instructive about the trace-element remobilization potentially associated with an abrupt boundary. Consequently, the applied methodology (LA-ICP-MS analyses in continuous mode after resin embedding) is adequate for advanced studies of abrupt boundaries such as the KPgB, enhancing time resolution while also detecting the distinctly different pacing of elemental peaks.

Acknowledgments

This research was funded through Projects CGL2012-33281, CGL2012-32659, CGL2015-66835, and CGL2015-66830, Project RNM-05212 (Secretaría de Estado de I + D + I, Spain), Research Groups RNM-178 and RNM-179 (Junta de Andalucía) and FEDER funds. The research of Sosa-Montes de Oca was supported by a pre-doctoral fellowship from the Spanish Ministry, MINECO. We are likewise grateful to Elisa Holanda for laboratory assistance at University of Granada and Amalia Filippidi, Anne Roepert and Alejandra Morera Chavarria for their help during the resin-embedding process at Utrecht University. Furthermore, we acknowledge access to the LA-ICP-MS facility at Geociencias-Utrecht and in particular the skillful assistance of Helen de Waard during the LA-ICP-MS analysis, and thank Rick Hennekam for his valuable advice on data processing. SEM-analyses were performed at the Centre for

Scientific Instrumentation (CIC), University of Granada (Spain). The manuscript greatly benefited from valuable comments and suggestions made by editor Tomas Algeo and reviewers Eustoquio Molina, Steve Goderis, and an anonymous 3rd reviewer.

References

- Aitchison, J., Egozcue, J., 2005. Compositional data analysis: where are we and where should we be heading? *Math. Geol.* 37, 829–850.
- Alegret, L., Thomas, E., 2005. Cretaceous/Paleogene boundary bathyal paleo-environments in the central North Pacific (DSDP site 465), the Northwestern Atlantic (ODP site 1049), the Gulf of Mexico and the Tethys: the benthic foraminiferal record. *Palaeogeogr. Palaeoclimatol. Palaeoecol.* 224, 53–82.
- Alegret, L., Thomas, E., 2009. Food supply to the seafloor in the Pacific Ocean after the Cretaceous/Paleogene boundary event. *Mar. Micropaleontol.* 73, 105–116.
- Alegret, L., Thomas, E., 2013. Benthic foraminifera across the Cretaceous/Paleogene boundary in the Southern Ocean (ODP site 690): diversity, food and carbonate saturation. *Mar. Micropaleontol.* 105, 40–51.
- Alegret, L., Thomas, E., Lohmann, K.C., 2012. End-Cretaceous marine mass extinction not caused by productivity collapse. *Proc. Natl. Acad. Sci. U. S. A.* 109, 728–732.
- Alvarez, L.W., Alvarez, W., Asaro, F., Michel, H.V., 1980. Extraterrestrial cause for the Cretaceous-Tertiary Extinction. *Science* 208, 1095–1108 (80-).
- Arenillas, I., Arz, J., Molina, E., 2004. A new high-resolution planktic foraminiferal zonation and subzonation for the lower Danian. *Lethaia* 37, 79–95.
- Artemieva, N., Morgan, J., 2009. Modeling the formation of the K-Pg boundary layer. *Icarus* 201, 768–780.
- Arz, J.A., Arenillas, I., Molina, E., Sepúlveda, R., 2000. La estabilidad evolutiva de los foraminíferos planctónicos en el Maastrichtense Superior y su extinción en el límite Cretácico/Terciario de Caravaca, España. *Rev. Geol. Chile* 27.
- Belza, J., Goderis, S., Smit, J., Vanhaecke, F., Baert, K., Terryn, H., Claeys, P., 2015. High spatial resolution geochemistry and textural characteristics of “microtektite” glass spherules in proximal Cretaceous-Paleogene sections: insights into glass alteration patterns and precursor melt lithologies. *Geochim. Cosmochim. Acta* 152, 1–38.
- Belza, J., Goderis, S., Montanari, A., Vanhaecke, F., Claeys, P., 2017. Petrography and geochemistry of distal spherules from the K-Pg boundary in the Umbria-Marche region (Italy) and their origin as fractional condensates and melts in the Chicxulub impact plume. *Geochim. Cosmochim. Acta* 202, 231–263.
- Berglund, M., Wieser, M.E., 2011. Isotopic compositions of the elements 2009 (IUPAC technical report). *Pure Appl. Chem.* 83, 397–410.
- Berndt, J., Deutsch, A., Schulte, P., Mezger, K., 2011. The Chicxulub ejecta deposit at Demerara Rise (western Atlantic): dissecting the geochemical anomaly using laser ablation-mass spectrometry. *Geology* 39, 279–282.
- Birch, H.S., Coxall, H.K., Pearson, P.N., Kroon, D., Schmidt, D.N., 2016. Partial collapse of the marine carbon pump after the Cretaceous-Paleogene boundary. *Geology* 44, 287–290.
- Brinkhuis, H., Smit, J., 1996. The Geulhemmerberg Cretaceous/Tertiary boundary section (Maastrichtian type area, SE Netherlands): an introduction. *Geol. Mijnb.* 75, 101–106.
- Brugger, J., Feulner, G., Petri, S., 2017. Baby, it's cold outside: climate model simulations of the effects of the asteroid impact at the end of the Cretaceous. *Geophys. Res. Lett.* 44.
- Calvert, S.E., Pedersen, T.F., 1993. Geochemistry of recent oxic and anoxic marine sediments: implications for the geological record. *Mar. Geol.* 113, 67–88.
- Canudo, J.I., Keller, G., Molina, E., 1991. Cretaceous/Tertiary boundary extinction pattern and faunal turnover at Agost and Caravaca, S.E. Spain. *Mar. Micropaleontol.* 17, 319–341.
- Esmeray-Senlet, S., Wright, J.D., Olsson, R.K., Miller, K.G., Browning, J.V., Quan, T.M., 2015. The Cretaceous/Paleogene mass extinction. *Paleoceanography* 30, 718–738.
- Galeotti, S., Brinkhuis, H., Huber, M., 2004. Records of post-Cretaceous-Tertiary boundary millennial-scale cooling from the western Tethys: a smoking gun for the impact-winter hypothesis? *Geology* 32, 529–532.
- Goderis, S., Tagle, R., Belza, J., Smit, J., Montanari, A., Vanhaecke, F., Erzinger, J., Claeys, P., 2013. Reevaluation of siderophile element abundances and ratios across the Cretaceous-Paleogene (K-Pg) boundary: implications for the nature of the projectile. *Geochim. Cosmochim. Acta* 120, 417–446.
- Groot, J.J., de Jonge, R.B.G., Langereis, C.G., ten Kate, W.G.H.Z., Smit, J., 1989. Magnetostratigraphy of the Cretaceous-Tertiary boundary at Agost (Spain). *Earth Planet. Sci. Lett.* 94, 385–397.
- Günther, D., Audéat, A., Frischknecht, R., Heinrich, C.A., 1998. Quantitative analysis of major, minor and trace elements in fluid inclusions using laser ablation – inductively coupled plasma mass spectrometry. *J. Anal. At. Spectrom.* 13, 263–270.
- Hennekam, R., Jilbert, T., Mason, P.R.D., de Lange, G.J., Reichart, G.J., 2015. High-resolution line-scan analysis of resin-embedded sediments using laser ablation-inductively coupled plasma-mass spectrometry (LA-ICP-MS). *Chem. Geol.* 403, 42–51.
- Hull, P., 2015. Life in the aftermath of mass extinctions. *Curr. Biol.* 25, R941–R952.
- Ibáñez-Insa, J., Pérez-Cano, J., Fondevilla, V., Oms, O., Rojas, M., Fernández-Turiel, J.L., Anadón, P., 2017. Portable X-ray fluorescence identification of the Cretaceous/Paleogene boundary: application to the Agost and Caravaca sections, SE Spain. *Cretac. Res.* 78, 139–148.
- Jenner, F.E., Arevalo, R.D., 2016. Major and trace element analysis of natural and experimental igneous systems using LA-ICP-MS. *Elements* 12, 311–316.
- Jilbert, T., de Lange, G., Reichart, G.J., 2008. Fluid displacive resin embedding of laminated sediments: preserving trace metals for high-resolution paleoclimate investigations. *Limnol. Oceanogr. Methods* 6, 16–22.

- Jochum, K.P., Weis, U., Stoll, B., Kuzmin, D., Yang, Q., Raczek, I., Jacob, D.E., Stracke, A., Birbaum, K., Frick, D.A., Günther, D., Enzweiler, J., 2011. Determination of reference values for NIST SRM 610-617 glasses following ISO guidelines. *Geostand. Geoanal. Res.* 35, 397–429.
- Kaiho, K., Oshima, N., Adachi, K., Adachi, Y., Mizukami, T., Fujibayashi, M., Saito, R., 2016. Global climate change driven by soot at the K-Pg boundary as the cause of the mass extinction. *Sci. Rep.* 6, 28427.
- Korbar, T., Montanari, A., Fucek, V.P., Fucek, L., Coccioni, R., McDonald, I., Claeys, P., Schulz, T., Koeberl, C., 2015. Potential Cretaceous-Paleogene boundary tsunami deposit in the intra-Tethyan Adriatic carbonate platform section of Hvar (Croatia). *Bull. Geol. Soc. Am.* 127, 1666–1680.
- Kring, D.A., 2007. The Chicxulub impact event and its environmental consequences at the Cretaceous-Tertiary boundary. *Palaeogeogr. Palaeoclimatol. Palaeoecol.* 255, 4–21.
- Laska, W., Rodríguez-Tovar, F.J., Uchman, A., 2017. Evaluating macrobenthic response to the Cretaceous–Palaeogene event: a high-resolution ichnological approach at the Agost section (SE Spain). *Cretac. Res.* 70, 96–110.
- Loroch, D., Deutsch, A., Berndt, J., Bornemann, A., 2016. The Cretaceous/Paleogene (K-Pg) boundary at the J Anomaly Ridge, Newfoundland (IODP Expedition 342, Hole U1403B). *Meteorit. Planet. Sci.* 51, 1370–1385.
- MacLeod, N., Keller, G., 1991. Hiatus distributions and mass extinctions at the Cretaceous/Tertiary boundary. *Geology* 19, 497–501.
- Martínez-Ruiz, F., Ortega-Huertas, M., Palomo, I., 1999. Positive Eu anomaly development during diagenesis of the K/T boundary ejecta layer in the Agost section (SE Spain): implications for trace-element remobilization. *Terra Nov.* 11, 290–296.
- Martínez-Ruiz, F., Ortega-Huertas, M., Kroon, D., Smit, J., Palomo-Delgado, I., Rocchia, R., 2001. Geochemistry of the Cretaceous-Tertiary boundary at Blake Nose (ODP leg 171B). *Geol. Soc. Lond. Spec. Publ.* 183, 131–148.
- Molina, E., 2015. Evidence and causes of the main extinction events in the Paleogene based on extinction and survival patterns of foraminifera. *Earth Sci. Rev.* 140, 166–181.
- Molina, E., Arenillas, I., Arz, J.A., 1996. The Cretaceous/Tertiary boundary mass extinction in planktic foraminifera at Agost, Spain. *Rev. Micropaleontol.* 39, 225–243.
- Molina, E., Arenillas, I., Arz, J.A., 1998. Mass extinction in planktic foraminifera at the Cretaceous/Tertiary boundary in subtropical and temperate latitudes. *Bull. Soc. Geol. Fr.* 169, 351–363.
- Molina, E., Alegret, L., Arenillas, I., Arz, J.A., 2005. The Cretaceous/Paleogene boundary at the Agost section revisited: paleoenvironmental reconstruction and mass extinction pattern. *J. Iber. Geol.* 31, 135–148.
- Ortega-Huertas, M., Martínez-Ruiz, F., Acquafredda, P., Palomo, I., 1994. Platinum-group elements in the cores of potassium feldspar spherules from the cretaceous-tertiary boundary at caravaca (Spain). *Estud. Geol.* 7, 3–7.
- Ortega-Huertas, M., Martínez-Ruiz, F., Palomo, I., Charnley, H., 1995. Comparative mineralogical and geochemical clay sedimentation in the Betic Cordilleras and Basque-Cantabrian Basin areas at the Cretaceous-Tertiary boundary. *Sediment. Geol.* 94, 209–227.
- Ortega-Huertas, M., Martínez-Ruiz, F., Palomo, I., Charnley, H., 2002. Review of the mineralogy of the Cretaceous-Tertiary boundary clay: evidence supporting a major extraterrestrial catastrophic event. *Clay Miner.* 37, 395–411.
- van Os, B.J.H., Middelburg, J.J., de Lange, G.J., 1991. Possible diagenetic mobilization of barium in sapropelic sediment from the eastern Mediterranean. *Mar. Geol.* 100, 125–136.
- Peryt, D., Alegret, L., Molina, E., 2002. The Cretaceous/Paleogene (K/P) boundary at Ain Settar, Tunisia: restructuring of benthic foraminiferal assemblages. *Terra Nova* 14, 101–107.
- Preisinger, A., Aslanian, S., Brandstätter, F., Grass, F., Stradner, H., Summesberger, H., 2002. Cretaceous-Tertiary profile, rhythmic deposition, and geomagnetic polarity reversals of marine sediments near Bjala, Bulgaria. *Geol. Soc. Am. Spec. Pap.* 356, 213–229.
- Reitz, A., Thomson, J., De Lange, G.J., Hensen, C., 2006. Source and development of large manganese enrichments above eastern Mediterranean sapropel S1. *Paleoceanography* 21, 1–17.
- Renne, P.R., Deino, A.L., Hilgen, F.J., Kuiper, K.F., Mark, D.F., Mitchell, W.S., Morgan, L.E., Mundil, R., Smit, J., 2013. Time scales of critical events around the Cretaceous-Paleogene boundary. *Science* 339, 684–687.
- Ritter, X., Deutsch, A., Berndt, J., Robin, E., 2015. Impact glass spherules in the Chicxulub K-Pg event bed at Beloc, Haiti: alteration patterns. *Meteorit. Planet. Sci.* 50, 418–432. <http://dx.doi.org/10.1111/maps.12432>.
- Rodríguez-Tovar, F.J., 2005. Fe-oxide spherules infilling *Thalassinoides* burrows at the Cretaceous-Paleogene (K-P) boundary: evidence of a near-contemporaneous macrobenthic colonization during the K-P event. *Geology* 33, 585.
- Rodríguez-tovar, J., Uchman, A., 2004a. Trace fossils after the KT boundary event from the Agost section, SE Spain. *Geol. Mag.* 141, 429–440.
- Rodríguez-Tovar, F.J., Uchman, A., 2004b. Ichnotaxonomic analysis of the Cretaceous/Paleogene boundary interval in the Agost section, south-east Spain. *Cretac. Res.* 25, 635–647.
- Rodríguez-Tovar, F.J., Martínez-Ruiz, F., Bernasconi, S.M., 2004. Carbon isotope evidence for the timing of the Cretaceous-Paleogene macrobenthic colonisation at the Agost section (southeast Spain). *Palaeogeogr. Palaeoclimatol. Palaeoecol.* 203, 65–72.
- Rodríguez-Tovar, F.J., Martínez-Ruiz, F., Bernasconi, S.M., 2006. Use of high-resolution ichnological and stable isotope data for assessing completeness of a K-P boundary section, Agost, Spain. *Palaeogeogr. Palaeoclimatol. Palaeoecol.* 237, 137–146.
- Scasso, R.A., Concheyro, A., Aberhan, M., Hecht, L., Medina, F.A., Tagle, R., 2005. A tsunami deposit at the Cretaceous/Paleogene boundary in the Neuquén Basin of Argentina. *Cretac. Res.* 26, 283–297.
- Schueth, J.D., Bralower, T.J., Jiang, S., Patzkowsky, M.E., 2015. The role of regional survivor incumbency in the evolutionary recovery of calcareous nannoplankton from the Cretaceous/Paleogene (K/Pg) mass extinction. *Paleobiology* 41, 661–679.
- Schulte, P., Alegret, L., Arenillas, I., Arz, J.A., Barton, P.J., Bown, P.R., Bralower, T.J., Christeson, G.L., Claeys, P., Cockell, C.S., Collins, G.S., Deutsch, A., Goldin, T.J., Goto, K., Grajales-Nishimura, J.M., Grieve, R.A.F., Gulick, S.P.S., Johnson, K.R., Kiessling, W., Koeberl, C., Kring, D.A., MacLeod, K.G., Matsui, T., Melosh, H.J., Montanari, A., Morgan, J.V., Neal, C.R., Nichols, D.J., Norris, R.D., Pierazzo, E., Ravizza, G., Rebolledo-Vieyra, M., Reimold, W.U., Robin, E., Salge, T., Speijer, R.P., Sweet, A.R., Urrutia-Fucugauchi, J., Vajda, V., Whalen, M.T., Willumsen, P.S., 2010. The Chicxulub asteroid impact and mass extinction at the Cretaceous-Paleogene boundary. *Science* 327, 1214–1218 (80-).
- Sepúlveda, J., Wendler, J.E., Summons, R.E., Hinrichs, K.-U., 2009. Rapid resurgence of marine productivity after the Cretaceous-Paleogene mass extinction. *Science* 326, 129–132 (80-).
- Shonting, D., Ezrailson, C., 2017. *Chicxulub: The Impact and Tsunami*. Springer Praxis books.
- Shukolyukov, A., Lugmair, G.W., 1998. All use subject to JSTOR terms and conditions isotopic evidence for the Cretaceous-Tertiary impactor and its type. *Science* 282, 927–929 (80-).
- Smit, J., 1990. Meteorite impact, extinctions and the Cretaceous-Tertiary Boundary.pdf. *Geol. Mijnb.* 69, 187–204.
- Smit, J., 1999. The global stratigraphy of the cretaceous-tertiary boundary impact ejecta. *Annu. Rev. Earth Planet. Sci.* 27, 75–113.
- Smit, J., Hertogen, J., 1980. An extraterrestrial event at the Cretaceous-Tertiary boundary. *Nat. Geosci.* 285, 198–200.
- Smit, J., Klaver, G., 1981. Sanidine spherules at the Cretaceous-Tertiary boundary indicate a large impact event. *Nature* 292, 47–49.
- Sosa-Montes de Oca, C., Martínez-Ruiz, F., Rodríguez-Tovar, F.J., 2013. Bottom-water conditions in a marine basin after the cretaceous-paleogene impact event: timing the recovery of oxygen levels and productivity. *PLoS One* 8, e82242.
- Sosa-Montes de Oca, C., Rodríguez-Tovar, F.J., Martínez-Ruiz, F., 2016. Geochemical and isotopic characterization of trace fossil infillings: new insights on tracemaker activity after the K/Pg impact event. *Cretac. Res.* 57, 391–401.
- Sosa-Montes de Oca, C., Rodríguez-Tovar, F.J., Martínez-Ruiz, F., Monaco, P., 2017. Paleoenvironmental conditions across the Cretaceous–Paleogene transition at the Apennines sections (Italy): an integrated geochemical and ichnological approach. *Cretac. Res.* 71, 1–13.
- Sylvester, P.J., Jackson, S.E., 2016. A brief history of laser ablation inductively coupled plasma mass spectrometry (LA-ICP-MS). *Elements* 12, 307–310.
- Tribouillard, N., Algeo, T.J., Lyons, T., Riboulleau, A., 2006. Trace metals as paleoredox and paleoproductivity proxies: an update. *Chem. Geol.* 232, 12–32.
- Urrutia-Fucugauchi, J., Pérez-Cruz, L., 2016. Planetary sciences, geodynamics, impacts, mass extinctions, and evolution: developments and interconnections. *Int. J. Geophys.* 2016.
- Vellekoop, J., Sluijs, A., Smit, J., Schouten, S., Weijers, J.W.H., Sinninghe Damste, J.S., Brinkhuis, H., 2014. Rapid short-term cooling following the Chicxulub impact at the Cretaceous-Paleogene boundary. *Proc. Natl. Acad. Sci. U. S. A.* 1–5.
- Vellekoop, J., Smit, J., van de Schootbrugge, B., Weijers, J.W.H., Galeotti, S., Sinninghe Damste, J.S., Brinkhuis, H., 2015. Palynological evidence for prolonged cooling along the Tunisian continental shelf following the K-Pg boundary impact. *Palaeogeogr. Palaeoclimatol. Palaeoecol.* 426, 216–228.
- Vellekoop, J., Esmeray-Senlet, S., Miller, K.G., Browning, J.V., Sluijs, A., van de Schootbrugge, B., Sinninghe Damste, J.S., Brinkhuis, H., 2016. Evidence for Cretaceous-Paleogene boundary bolide “impact winter” conditions from New Jersey, USA. *Geology* 44, 619–622.
- Wagner, T., Fusswinkel, T., Wälle, M., Heinrich, C.A., 2016. Microanalysis of fluid inclusions in crustal hydrothermal systems using laser ablation methods. *Elements* 12, 323–328.
- Wang, Z., Hattendorf, B., Günther, D., 2006. Analyte response in laser ablation inductively coupled plasma mass spectrometry. *J. Am. Soc. Mass Spectrom.* 17, 641–651.
- Wilf, P., Johnson, K.R., Huber, B.T., 2003. Correlated terrestrial and marine evidence for global climate changes before mass extinction at the cretaceous-Paleogene boundary. *Proc. Natl. Acad. Sci.* 100, 599–604.
- Woelders, L., Vellekoop, J., Kroon, D., Smit, J., Casadío, S., Prámparo, M.B., Dinarès-Turell, J., Peterse, F., Sluijs, A., Lenaerts, J.T.M., Speijer, R.P., 2017. Latest Cretaceous Climatic and Environmental Change in the South Atlantic Region.